Bayesian Operational Modal Analysis with Buried Modes

Yi-Chen Zhu[1], Siu-Kui Au[2] and James Mark William Brownjohn[3]

Abstract

In full-scale ambient vibration tests, challenging situations exist where in the frequency domain the measured data is dominated by other modes that 'bury' the subject mode of interest. In this case, conventional modal identification methods are either not applicable or inefficient to apply. This paper proposes a Bayesian frequency domain method for identifying the modal properties of such buried modes. The buried-mode situation is modelled and computation difficulties are addressed, leading to an efficient algorithm for modal identification in such challenging situation. The proposed method is validated by synthetic data examples. The associated uncertainty of the identified modal parameters are investigated. The method is also applied to identifying the buried modes of a long-span suspension bridge, demonstrating its utility with challenging modes encountered in field test data.

Key Words: Ambient data; Bayesian methods; Buried mode; Operational modal analysis

1. Introduction

Ambient modal identification, conventionally known as 'operational modal analysis' (OMA), aims at identifying the modal properties (normally includes natural frequencies, damping ratios and mode shapes) of a structure under ambient excitation conditions [1]. OMA is a popular tool for assessing the in-situ modal properties of large scale civil infrastructure as it can be performed economically and efficiently under working conditions without artificial loading [2–4]. Ambient vibration test is becoming an important task in dynamic assessment of long-span bridges, e.g., early application on Golden Gate Bridge [5], long-term structural health monitoring of Tamar suspension bridge [6] and recent studies based on wireless

[1] Corresponding author. Institute for Risk and Uncertainty and Centre for Engineering Dynamics, University of Liverpool, UK. Email: sgyzhu7@liverpool.ac.uk.
[2] Professor, Chair of Uncertainty, Reliability and Risk, University of Liverpool, UK. Email: siukuiau@liverpool.ac.uk
[3] Professor of Structural Dynamics, University of Exeter, UK. E-mail: J.Brownjohn@Exeter.ac.uk

sensing systems [7,8]. It has also been widely used to investigate the dynamic properties of tall buildings subjected to strong winds [9–12].

OMA is an 'inverse' or 'backward' problem where one is interested in gaining knowledge about the instrumented structure based on measured response rather predicting the response based on assumed properties (as in a 'forward' problem). Methods have been developed in both non-Bayesian and Bayesian manner. Bayesian methods view probability as a measure of plausibility that depend explicitly on available information (data) and assumptions. Non-Bayesian methods view probability as a relative frequency of occurrence among conceptually repeated experiments. In OMA, non-Bayesian methods are conventional. Popular ones include stochastic subspace identification (SSI, time domain) [13–15] and frequency domain decomposition (FDD, frequency domain) [16]. Bayesian OMA methods are developed more recently and are less conventional. Methods based on different types of information have been developed, e.g., in the time domain [17] and in the frequency domain based on sample power spectral density (PSD) [18–20] and fast Fourier Transform (FFT) of measured data [21,22]. Among these, methods based on FFT are preferred as they do not involve averaging concepts (not so for PSD methods) and they allow one to make inference based on the FFT of a selected band around the subject mode (not possible in the time domain), which significantly simplifies the identification model and reduce the modelling error. See [23] for a recent monograph.

Under ambient excitations, the magnitude of different modal response cannot be actively controlled and this can lead to challenging situations. One well-recognised situation is that of an inadequately excited mode below instrument noise level, for which artificial means (e.g., shaker) is necessary if the mode is desired, or dismissed (if ever known) from the set of identified modes. Another situation, which is less commonly discussed but nevertheless relevant and shall be focussed in this work, is that of a 'buried mode'. In the frequency domain, even near the natural frequency of the mode of interest, the measured data is dominated by other modes. This renders conventional modelling and identification strategies inapplicable or inefficient. One typical case where buried-mode situation may occur is OMA with long-span bridges. The modal response in the vertical direction (mainly due to traffic) is often much larger than that in the transverse direction (mainly due to wind). When combined in a single data set, some transverse modes can be buried by vertical modes. To illustrate, Figure 1 shows the root PSD (power spectral density) spectrum calculated from a set of ambient data measured on a long-span bridge (see Section 6.3 for details later). Even in their

resonance bands, Mode 1 and Mode 2 (dominant in transverse direction with spectral peaks in solid lines) are 'buried' by their neighbouring modes (dominant in vertical direction with spectral peaks in dashed lines), whose spectral contributions are significant. Applying conventional frequency domain algorithms for well separated modes to identifying buried modes will incur significant modelling error because the unaccounted contribution from the burying modes cannot be modelled by simple prediction error models, e.g., independent and identically distributed (i.i.d.) among different measured degrees of freedom (DOFs).

Two intuitive strategies are often used to handle buried modes. One strategy is to select (i.e., use the FFT as data) a frequency band that includes spectral peaks of both the subject (buried) mode and the dominant (burying) mode; and identify them together using a multiple (possibly closely-spaced) mode algorithm [24]. One issue with this strategy is that the two modes need not be close, necessitating a very wide band that significantly increases the modelling error risk (e.g., due to the contribution of other modes or unmodeled coloured activities in the band) and causes bias in the identification results. Mode 2 in Section 6.3 is a typical example where additional spectral peaks can be found between the burying mode and Mode 2 itself, which leads to identification errors and even convergence problems for the multiple mode algorithm. Another intuitive strategy is to identify using only the data of those measured DOFs not dominated by the burying modes. In this case, algorithms for well-separated modes can be applied but the mode shape values in the excluded DOFs cannot be identified. Note also that this strategy is only feasible when the burying contribution appears only in the excluded DOFs, e.g., vertical DOFs for long-span bridges.

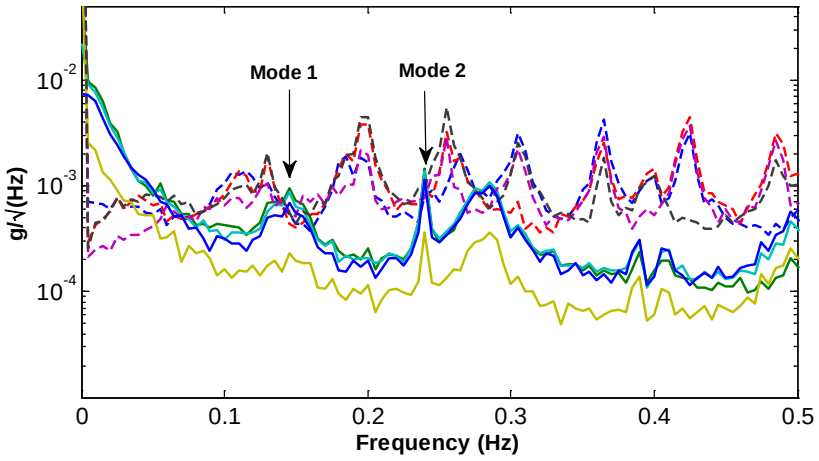

Figure 1. Root PSD Spectrum of Setup 1 (Dashed line: Vertical Direction; Solid Line: Transverse Direction; Details: See Section 6.3)

Motivated by the above considerations, this work proposes a Bayesian OMA method for buried mode capable of utilising all measured DOFs (i.e., no need to exclude DOFs), maintaining the efficiency of well-separated mode algorithms while avoiding modelling error from burying modes. The buried mode situation is modelled and the likelihood function for Bayesian inference is derived. A fast algorithm is then developed for efficiently determining the most probable values of modal parameters. The proposed method is validated and the identification uncertainty is investigated using synthetic data examples. The method is also applied to identifying the buried modes of a long-span bridge, where the applicability of the proposed method to field test data with challenging issues are discussed.

2. Modelling buried mode

The spectral characteristics of the buried mode and the burying mode are first investigated in this section. Focusing on the frequency range around the resonance peak of the buried mode, the theoretical PSD matrix for buried mode cases is modelled. Based on this model, the likelihood function is derived, which leads to the Bayesian OMA algorithm in the next section.

Let $\left\{\hat{\ddot{\mathbf{x}}}_j \in R^n\right\}_{j=1}^N$ denote the time histories of the measured ambient acceleration data with n measured DOFs and N samples per DOF. The 'scaled' FFT of $\left\{\hat{\ddot{\mathbf{x}}}_j\right\}$ is defined as:

$$\mathcal{F}_k = \sqrt{\frac{2\Delta t}{N}} \sum_{j=1}^{N} \hat{\ddot{\mathbf{x}}}_j \exp\left[-2\pi \mathbf{i} \frac{(k-1)(j-1)}{N}\right] \tag{1}$$

where $\mathbf{i}^2 = -1$ and Δt is the sampling interval. $\mathcal{F}_k$ corresponds to frequency $\mathrm{f}_k = (k-1)/N\Delta t\,(\mathrm{Hz})$ for $k = 1,...N_q$, where $N_q = \mathrm{int}(N/2)+1$ (int(.) denotes integer part) is the index corresponding to the Nyquist frequency. Without loss of generality, consider the FFT of data $\mathcal{F}_k$ dominated by two modes:

$$\mathcal{F}_k = \boldsymbol{\varphi}_1 \ddot{\eta}_{1k} + \boldsymbol{\varphi}_2 \ddot{\eta}_{2k} + \boldsymbol{\varepsilon}_k \tag{2}$$

where $\boldsymbol{\varphi}_1$ and $\boldsymbol{\varphi}_2$ denote the mode shape of the burying and the buried mode, respectively; $\ddot{\eta}_{1k}$ and $\ddot{\eta}_{2k}$ denote the corresponding FFT of modal acceleration; and $\boldsymbol{\varepsilon}_k$ is the scaled FFT of prediction error due to measurement noise or modelling error.

Assuming classically damped modes, the modal acceleration satisfies the modal equation of motion:

$$\ddot{\eta}_i(t) + 2\zeta_i\omega_i\dot{\eta}_i(t) + \omega_i^2\eta_i(t) = p_i(t) \qquad i = 1,2 \tag{3}$$

where $\omega_i = 2\pi f_i$ (rad/s); f_i (Hz), ζ_i and $p_i(t)$ are the natural frequency, damping ratio and modal force of the mode.

The modal force is modelled as a stationary process with a constant spectral density matrix; and prediction error as Gaussian white noise with a constant PSD, i.i.d. among the measured DOFs. The theoretical PSD is then given by

$$\mathbf{E}_k = E[\mathcal{F}_k\mathcal{F}_k^*] = \mathbf{\Phi}\mathbf{H}_k\mathbf{\Phi}^T + S_e\mathbf{I}_n \tag{4}$$

where $\mathbf{\Phi} = [\boldsymbol{\varphi}_1 \quad \boldsymbol{\varphi}_2] \in R^{n\times 2}$; S_e is the (constant) PSD of prediction error, $\mathbf{I}_n$ denotes the $n \times n$ identity matrix and $\mathbf{H}_k \in C^{2\times 2}$ is the theoretical PSD matrix of modal acceleration given by:

$$\mathbf{H}_k = diag(\mathbf{h}_k)\mathbf{S}diag(\mathbf{h}_k^*) \tag{5}$$

Here, $\mathbf{S}$ is the (constant) PSD matrix of modal forces, $\mathbf{h}_k \in C^2$ is the vector of modal frequency response function with

$$h_{ik} = \left[\left(\beta_{ik}^2 - 1\right) + \mathbf{i}\left(2\zeta\beta_k\right)\right]^{-1} \qquad \beta_{ik} = f_i/\mathrm{f}_k \tag{6}$$

and $diag(\mathbf{h}_k)$ denotes a diagonal matrix with the ith element equal to h_{ik}.

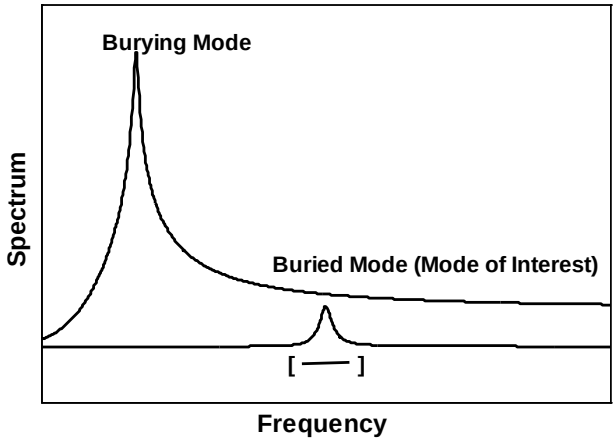

Figure 2. Schematic Diagram of Buried Mode Situation

The PSD matrix for modal acceleration in Eq.(4) holds for general multiple modes situation. To facilitate computation, it is now modified by taking account of the buried mode situation. Consider the frequency band around the resonance peak of the buried mode. The buried and burying modes are assumed to be well-separated, for otherwise they should be identified by existing closely-spaced modes algorithm [24]. The situation is illustrated in Figure 2. The symbol '[-]' denotes the selected frequency band, whose FFT data will be used for making Bayesian inference (entering into the likelihood function). Without loss of generality, the figure assumes that the burying mode appears on the left of the buried mode, for otherwise the magnitude of its transfer function (hence FFT of modal response) in the band is inversely proportional to the frequency separation and hence small (no burying situation). The fact that the selected band is at the tail of the burying mode leads to simplification of the modal frequency response function $\mathbf{h}_k$ in Eq.(6). When the burying mode is on the left-hand side of the mode of interest and is well apart, $h_{1k} \approx -1$ and $diag\left(\mathbf{h}_k\right)$ can be approximated as

$$diag\left(\mathbf{h}_k\right) \approx \begin{bmatrix} -1 & \\ & h_{2k} \end{bmatrix} \tag{7}$$

This is justified when $\left(f_1 / f_2\right)^2 \ll 1$. To see this, note that h_{1k} depends on f_1 through the term β_{1k}. Within the frequency band of interest, i.e., around the resonance peak of the buried mode, f_k is close to f_2 and hence $\beta_{1k} \approx f_1 / f_2$. For small damping, h_{1k} is dominant by the term $\left(\beta_{ik}^2 - 1\right)$ and $h_{1k} \approx -1$ when $\beta_{1k}^2 \ll 1$.

Since the natural frequency and damping ratio of the burying mode are reflected in the theoretical PSD matrix (hence likelihood function) of data through the term h_{1k} (which has now been approximated as -1), these properties are unlikely to be identifiable from the selected band. This is intuitive as the selected frequency band covers only the tail of the burying mode. This also implies that it is not possible to identify these two modes together using the original multiple mode algorithm [24] (e.g., the optimisation process for MPV will not converge) unless a wider frequency band involving the spectral peaks of both modes are used (which increases modelling error risk). On the other hand, using a conventional well-separated mode algorithm will lead to significant modelling error because the contribution of the burying mode cannot be accounted by a conventional prediction error model (e.g., i.i.d.) even when it is off-resonance in the selected band. The modal contribution of the burying

mode is significant among different DOFs and is neither independent nor identically distributed. The mode shape values of the burying mode $\boldsymbol{\varphi}_1$ are still involved in the theoretical PSD matrix $\mathbf{E}_k$ (see Eq. (4)). The identifiability observation in Eq.(7) leads one to use a simplified model (rather than the original two-mode model) for identifying the buried mode, where unidentifiable parameters (i.e., natural frequency and damping ratio of the burying mode) are excluded. At the same time, the frequency band does not need to be unnecessarily wide, which effectively reduces modelling error due to unaccounted activities.

Quantitatively, buried mode situation refers to the case when the modal contribution of one mode is larger than the modal contribution of the mode of interest in the selected frequency band. In this case, the former is considered as the burying mode and the latter is considered as the buried mode. In practice, the most direct way is to examine the singular value spectrum (i.e., the plot of eigenvalues of the PSD matrix $\mathbf{E}_k$). Figure 2 is a typical look of the singular value spectrum for a buried mode situation. When there are significant eigenvalues that are larger than the spectral peak of the mode of interest, the effect of such modal contribution cannot be neglected and buried mode situation should be considered.

3. Bayesian algorithm for most probable value

Based on the theoretical PSD matrix for the buried mode in the last section, a Bayesian OMA method is developed in this section. For notational simplicity, the mode index i is omitted in the following sections. The natural frequency and damping ratio of the buried mode will be abbreviated as f and ζ, respectively. Let $\{\mathcal{F}_k\}$ denote the set of FFT data in the selected frequency band used for modal identification with N_f points; and $\boldsymbol{\theta}$ denote the set of modal parameters to be identified (see Section 3.2 later for details). Using Bayes' theorem and assuming a uniform prior distribution, the posterior probability density function (PDF) of $\boldsymbol{\theta}$ given $\{\mathcal{F}_k\}$ is proportional to the likelihood function, i.e., $p(\boldsymbol{\theta}|\{\mathcal{F}_k\}) \propto p(\{\mathcal{F}_k\}|\boldsymbol{\theta})$. For high sampling rate and long data duration, it is a standard result in signal processing that $\{\mathcal{F}_k\}$ are asymptotically independent at different frequencies and jointly 'complex Gaussian' [25]. The likelihood function then can be given by

$$p(\{\mathcal{F}_k\}|\boldsymbol{\theta}) = (\pi)^{-nN_f} \times \prod_k (\det \mathbf{E}_k)^{-1} \exp\left[-\sum_k \mathcal{F}_k^* \mathbf{E}_k^{-1} \mathcal{F}_k \right] \tag{8}$$

where '*' denotes conjugate transpose and $\mathbf{E}_k = E[\mathcal{F}_k \mathcal{F}_k^* | \boldsymbol{\theta}]$ is the theoretical PSD matrix. For analysis or computation, it is more convenient to write:

$$p(\boldsymbol{\theta} | \{\mathcal{F}_k\}) \propto \exp[-L(\boldsymbol{\theta})] \tag{9}$$

where

$$L(\boldsymbol{\theta}) = \sum_k \ln \det \mathbf{E}_k + \sum_k \mathcal{F}_k^* \mathbf{E}_k^{-1} \mathcal{F}_k \tag{10}$$

is the 'negative log-likelihood function' (NLLF). For sufficient data, modal identification problem is 'globally identifiable' [26]. The most probable value (MPV) of $\boldsymbol{\theta}$ can be determined by maximising the posterior PDF, or equivalently minimising the NLLF with respect to $\boldsymbol{\theta}$.

Brute-force numerical optimisation of the NLLF is not feasible as the measured DOFs n can be moderate or large in real applications. Similar to other Bayesian FFT approaches, analytically resolving the dependence and singularity of the determinant and inverse of $\mathbf{E}_k$ on the mode shape is the key to developing an efficient algorithm for the buried mode.

The theoretical PSD matrix $\mathbf{E}_k$ for buried mode involves the mode shape matrix $\boldsymbol{\Phi}$ (see Eq.(4)), which is similar to that in general multiple mode cases. To suppress the growth of computation effect when optimising the NLLF, the mode shape matrix $\boldsymbol{\Phi}$ is expressed through an orthonormal basis. Assume that the mode shape subspace has a dimension of 2, for otherwise the two mode shapes are not distinguishable. Define an orthonormal basis $\mathbf{B} = [\mathbf{B}' \quad \mathbf{B}'_\perp] \in R^{n \times n}$, where $\mathbf{B}' \in R^{n \times 2}$ is an orthonormal basis spanning the mode shape subspace and $\mathbf{B}'_\perp \in R^{n \times (n-2)}$ is an orthonormal basis in the orthogonal complement of $\mathbf{B}'$. The mode shape matrix now can be represented as

$$\boldsymbol{\Phi} = \mathbf{B}' \boldsymbol{\alpha} \tag{11}$$

where $\boldsymbol{\alpha} \in R^{2 \times 2}$ is the coordinate matrix of $\boldsymbol{\Phi}$ with respect to basis $\mathbf{B}'$. Using the orthonormal properties of $\mathbf{B}'$, it can be shown that [24] the determinant and inverse of $\mathbf{E}_k$ are

$$\det \mathbf{E}_k = \det \mathbf{B} \det \mathbf{E}'_k \det S_e \mathbf{I}_{n-2} \det \mathbf{B}^T = {S_e}^{n-2} \det \mathbf{E}'_k \tag{12}$$

$$\mathbf{E}_k^{-1} = {S_e}^{-1} \mathbf{I}_n - S_e^{-1} \mathbf{B}' \left(\mathbf{I}_2 - S_e {\mathbf{E}'_k}^{-1} \right) \mathbf{B}'^T \tag{13}$$

where $\mathbf{E}'_k$ can be considered as a condensed form of $\mathbf{E}_k$ given by

$$\mathbf{E}'_k = \boldsymbol{\alpha} \mathbf{H}_k \boldsymbol{\alpha}^T + S_e \mathbf{I}_2 \tag{14}$$

Substituting into the NLLF in Eq.(10), the NLLF now can be expressed as:

$$\begin{aligned} L(\boldsymbol{\theta}) = {} & (n-2) N_f \ln S_e + {S_e}^{-1} d + \sum_k \ln \left(\det \mathbf{E}'_k \right) \\ & - S_e^{-1} \sum_k \mathcal{F}_k^* \mathbf{B}' \left(\mathbf{I}_2 - S_e {\mathbf{E}'_k}^{-1} \right) \mathbf{B}'^T \mathcal{F}_k \end{aligned} \tag{15}$$

where

$$d = \mathcal{F}_k \mathcal{F}_k^* \tag{16}$$

The dimension of the matrix computation involved in the NLLF (i.e., $\mathbf{E}'_k$) is now 2, which is much smaller than n in the initial expression. The mode shape basis has also been segregated out in the NLLF and can now be optimised through the last (quadratic) term in Eq.(15) with orthonormal constraints.

An efficient iterative algorithm is proposed in Section 3.1 to optimise the mode shape matrix using the Caley Transform [27] to preserve the orthonormal constraint. The remaining parameters then can be obtained based on the MPV of mode shape basis (see Section 3.2), and vice versa, which leads to an iterative algorithm. Proper parameterisation schemes are also proposed to preserve the constraints on the remaining parameters so that their MPV can be determined through unconstrained optimisation.

3.1 Most probable mode shape basis by Caley transformation

The NLLF in Eq.(15) depends on the mode shape basis $\mathbf{B}'$ through the last (quadratic) term. The MPV of $\mathbf{B}'$ should be obtained by minimising the latter, which can be written as

$$L_q = -S_e^{-1} \sum_k \mathcal{F}_k^* \mathbf{B}' \left(\mathbf{I}_2 - S_e {\mathbf{E}'_k}^{-1} \right) \mathbf{B}'^T \mathcal{F}_k \tag{17}$$

subjecting to constraint

$$\mathbf{B}'^{T}\mathbf{B}' = \mathbf{I}_2 \tag{18}$$

This is an optimisation problem with orthogonality constraints. In the Bayesian multi-mode algorithm [24], a rotation matrix is proposed to take care of the orthonormal constraints and $\mathbf{B}'$ is updated through Newton iteration. However, this requires proper parameterisation of the free angles in the rotation matrix. The gradient and Hessian of L_q with respect to these free angles also need to be derived, which cannot be expressed in concise forms. To address these issues, $\mathbf{B}'$ is determined through the Cayley transformation, which is also known as a type of Crank-Nicolson-like updating scheme [28]. It has been widely applied in solving inverse eigenvalue problems [29], heat equations and partial differential equations [30]. With proper step size, it is found that the Cayley transformation can also provide an efficient strategy for solving optimisation problems with orthogonality constraints [27]. Specifically, $\mathbf{B}'$ can be updated by

$$\mathbf{B}'_{updated} = \left(\mathbf{I} + \frac{\tau}{2}\mathbf{D}\right)^{-1}\left(\mathbf{I} - \frac{\tau}{2}\mathbf{D}\right)\mathbf{B}' \tag{19}$$

where τ is the step size and

$$\mathbf{D} = \mathbf{G}\mathbf{B}'^{T} - \mathbf{B}'\mathbf{G}^{T} \tag{20}$$

Here, $\mathbf{G}$ is the gradient of L_q with respect to $\mathbf{B}'$ given by

$$\mathbf{G} = -2S_e^{-1}\,\mathrm{Re}\left[\sum_k \mathcal{F}_k\mathcal{F}_k^{*}\mathbf{B}'\left(\mathbf{I}_2 - S_e\mathbf{E}_k'^{-1}\right)\right] \tag{21}$$

Eq.(19) is the closed form expression of the new trial point based on the Crank-Nicolson-like updating scheme with orthogonality constraints. It can be obtained as an extension of finding the p-harmonic flow [31]. Detailed derivation (see [27]) is omitted as it is out of the scope of this paper. The Barzilai-Borwein step size [32] is used in this work for τ to guarantee convergence with nearly no extra cost. Compared to the rotation matrix method, this updating scheme does not require parameterisation of free angles and the Hessian matrix of L_q. The MPV of mode shape basis now can be efficiently determined given the remaining parameters.

3.2 Most probable spectral parameters

Despite the mode shape basis, the remaining parameters include $f, \zeta, \mathbf{S}, \boldsymbol{\alpha}$ and S_e. Some parameters are subjected to constraints. Instead of incorporating these constraints into the optimisation procedure through numerical techniques (e.g., Lagrange multiplier), it is more

convenient to propose a parameterisation scheme that can automatically take care of the constraints. This issue has been investigated before and the approach here follows [24].

The mode shape coordinate matrix $\boldsymbol{\alpha}$ is subjected to the unit norm constraint inherited from the mode shape matrix $\boldsymbol{\Phi}$, i.e.,

$$\boldsymbol{\alpha}(i)^T \boldsymbol{\alpha}(i) = \boldsymbol{\alpha}(i)^T \mathbf{B}'^T \mathbf{B}' \boldsymbol{\alpha}(i) = \boldsymbol{\Phi}(i)^T \boldsymbol{\Phi}(i) = \left\| \boldsymbol{\Phi}(i) \right\|^2 = 1 \tag{22}$$

where $\boldsymbol{\alpha}(i)$ and $\boldsymbol{\Phi}(i)$ denote the i-th column of matrix $\boldsymbol{\alpha}$ and $\boldsymbol{\Phi}$, respectively. A parameterisation scheme is adopted that transfers the scaling of the modal force PSD to $\boldsymbol{\alpha}$ such that the resulting parameters are unconstrained. Specifically, define

$$\boldsymbol{\alpha}_s = \boldsymbol{\alpha} \sqrt{diag(\mathbf{S})} = \left[\sqrt{S_{11}} \boldsymbol{\alpha}(1) \quad \sqrt{S_{22}} \boldsymbol{\alpha}(2) \right] \tag{23}$$

Substituting into $\mathbf{E}'_k$ in Eq.(14) gives

$$\mathbf{E}'_k = \boldsymbol{\alpha}_s \mathbf{H}'_k \boldsymbol{\alpha}_s^T + S_e \mathbf{I}_2 \tag{24}$$

where

$$\mathbf{H}'_k = diag(\mathbf{h}_k) \mathbf{S}' diag(\mathbf{h}_k^*) \tag{25}$$

Here, $\mathbf{S}'$ is the dimensionless form of modal force PSD matrix with diagonal elements equal to 1 and off-diagonal elements equal to the coherence between the modal forces of the burying and buried modes, i.e.,

$$\mathbf{S}' = \begin{bmatrix} 1 & \chi \\ \bar{\chi} & 1 \end{bmatrix} \tag{26}$$

where

$$\chi = \frac{S_{12}}{\sqrt{S_{11} S_{22}}} \tag{27}$$

The coherence χ is subjected to the constraint $|\chi| \le 1$. For numerical optimisation, this constraint can be preserved by representing χ in terms of the angle $\{u, v\}$ such that:

$$\chi = \sin u \exp(\mathbf{i}v) \tag{28}$$

Based on the foregoing parameterisation, the unconstrained parameters $\boldsymbol{\alpha}_s$ and $\{u, v\}$ are used through the optimisation procedure in place of $\boldsymbol{\alpha}$ and $\mathbf{S}$. After obtaining the MPV of $\boldsymbol{\alpha}_s$ and $\{u, v\}$, the latter can be recovered. Specifically,

$$\hat{\boldsymbol{\alpha}}(i) = \frac{\hat{\boldsymbol{\alpha}}_s(i)}{\left\|\hat{\boldsymbol{\alpha}}_s(i)\right\|} \tag{29}$$

$$S_{ii} = \left\|\hat{\boldsymbol{\alpha}}_s(i)\right\|^2 \tag{30}$$

for $i = 1, 2$ and

$$\hat{S}_{12} = \sqrt{\hat{S}_{11}\hat{S}_{22}} \sin \hat{u} \exp(\mathbf{i}\hat{v}) \tag{31}$$

Here, a hat '^' denotes MPV.

4. Initial guess of modal parameters

In this section, proper initial guess of modal parameters for the iterative procedure is investigated. This is mainly based on the asymptotic characteristics of the MPV of modal parameters when the PSD of modal responses is much larger than that of the prediction error (i.e., high signal-to-noise ratio) within the selected frequency band. It can be shown that the asymptotic MPV of $\mathbf{B}'$ and S_e can be obtained analytically and the remaining parameters can also be empirically determined given the measured data or nominally assigned. The results are similar to the case of closely-spaced modes [24] so detailed derivations are omitted in this section.

The high signal-to-noise ratio condition refers to the case when

$$\mathbf{I}_2 - S_e \mathbf{E}_k'^{-1} \approx \mathbf{I}_2 \tag{32}$$

In this context, L_q in Eq.(17) can be expressed as:

$$\begin{aligned} L_q &\approx -S_e^{-1} \sum_k \mathcal{F}_k^* \mathbf{B}' \mathbf{B}'^T \mathcal{F}_k \\ &= -S_e^{-1} \left[\mathbf{B}'(1)^T \mathbf{D} \mathbf{B}'(1) + \mathbf{B}'(2)^T \mathbf{D} \mathbf{B}'(2) \right] \end{aligned} \tag{33}$$

where

$$\mathbf{D} = \sum_k \mathbf{D}_k = \sum_k \mathcal{F}_k^* \mathcal{F}_k \tag{34}$$

Due to the orthonormal properties of $\mathbf{B}'$ (i.e., $\mathbf{B}'(i)^T \mathbf{B}'(j) = \delta_{ij}$ for $i, j = 1, 2$), it is easy to show that the quadratic term in Eq.(33) is maximised (hence L_q is minimised) when $\mathbf{B}'(1)$ and $\mathbf{B}'(2)$ are the eigenvectors of $\mathbf{D}$ corresponding to the first two largest eigenvalues (normalised to unit norm).

The initial guess of prediction error S_e can also be obtained based on the high signal-to-noise ratio asymptotic. The condensed form of theoretical PSD matrix $\mathbf{E}_k'$ in Eq.(14) is dominated by the modal responses under high signal-to-noise condition and hence asymptotically independent of S_e. The NLLF now depends on S_e through the terms without $\mathbf{E}_k'$, which can be rewritten as

$$L(\boldsymbol{\theta}) = (n-2) N_f \ln S_e + S_e^{-1} (d - d') + (\text{terms do not depend on } S_e) \tag{35}$$

where

$$d' = \sum_k \mathcal{F}_k^* \mathbf{B}' \mathbf{B}'^T \mathcal{F}_k \tag{36}$$

The NLLF are of the form $\ln x + a/x$ in terms of S_e. This form has a unique minimum of $1 + \ln a$ at $x = a$. This yields the asymptotic MPV of S_e as:

$$\hat{S}_e \approx \frac{d - d'}{(n-2) N_f} \tag{37}$$

The initial guess of modal force PSD matrix $\mathbf{S}$ can be empirically obtained by noting that around the resonant frequency of the mode, the first two largest eigenvalues of $\mathbf{D}_k$ in Eq.(34) are approximately equal to S_{11} and $S_{22} / 4\zeta^2$. By nominally assuming the damping ratio of the mode of interest as 1%, S_{22} can be roughly estimated.

The initial guess of the remaining parameters can be nominally assigned. The initial guess for the natural frequency f can be simply picked from the spectral peak of the mode of interest in the singular value spectrum. The initial guess for damping ratio can be nominally assumed as 1% (say). The angles of the coherence value $\{u, v\}$ can be nominally assigned as 0.1, say.

The initial guess of the mode shape coordinate matrix $\boldsymbol{\alpha}$ can be assigned as 1 for diagonal terms and small random values for off-diagonal terms. The unconstrained parameter $\boldsymbol{\alpha}_s$ then can be calculated in terms of the initial guess of $\boldsymbol{\alpha}$ and $\{S_{ii}\}$ using Eq.(23).

5. Summary of procedure

Based on the foregoing analysis, an iterative procedure is proposed to determine the MPV of modal parameters for buried mode. Instead of optimising all the parameters simultaneously, the proposed method optimises them in groups (given the remaining parameters) and iterate until convergence. The convergence tolerance in the iteration can be set as 10^{-3} (say) on a fractional basis for all parameters. The iterative scheme is summarised as follows:

1) Calculate the FFT of the measured data and plot the singular value spectrum.
2) Select the frequency band for the mode of interest.
3) Calculate the initial guess for $f, \zeta, \boldsymbol{\alpha}_s, u, v, S_e$ and $\mathbf{B}'$ according to Section 4.
4) Update $\boldsymbol{\alpha}_s$ and u by minimising L in Eq.(15).
5) Update v by minimising L in Eq.(15).
6) Update f and ζ by minimising L in Eq.(15).
7) Update S_e by minimising L in Eq.(15).
8) Update $\mathbf{B}'$ using Eq.(19).

Repeat Step 4 to 8 until convergence.

After determining the MPVs of $\boldsymbol{\alpha}_s, u, v$ and $\mathbf{B}'$, the MPV of $\boldsymbol{\alpha}$ can be obtained using Eq.(29) and the MPV of $\mathbf{S}$ can be obtained using Eq.(30) and Eq.(31). The MPV of mode shape can be obtained based on the MPV of $\mathbf{B}'$ and $\boldsymbol{\alpha}$ by

$$\hat{\boldsymbol{\varphi}} = \hat{\mathbf{B}}'\hat{\boldsymbol{\alpha}} \tag{38}$$

6. Illustrative examples

Three examples are presented to illustrate the proposed method. The first example is based on synthetic data, which serves to verify the consistency of the method. The identification uncertainty is also discussed in this example. The identification quality of modal parameters

under different modal force PSDs of the burying mode are investigated in the second example based on a parametric study. In the third example, the proposed method is applied to modal analysis of field test ambient data measured on a long-span bridge. Modal identification focuses on two buried modes encountered in the measured data, where identification results are compared with those based on conventional methods that assume multiple modes with a wide frequency band and single mode around the resonance peak of the buried modes using data channels in the buried direction only. Challenges in field test conditions are also discussed.

6.1 Synthetic data (validation)

Consider a structure with six DOFs. Two modes are assumed for this structure with natural frequencies of 1Hz and 5Hz, respectively (while the other four modes are not considered when generating the synthetic data). The damping ratios of these two modes are assumed to be 1%. The mode shapes of these two modes (see Figure 3) are set to be $[1,2,3,4,5,6]^T$ and $[3,5,4,1,-2,-5]^T$ respectively (simulating shear building behaviour) and normalised to unit norm (i.e., sum of squares equal to 1). The first mode is the burying one subjected to a white noise modal force with a PSD of $1\times10^{-8}\mathrm{g}^2/\mathrm{Hz}$. The second mode is the buried one subjected to a white noise force with a PSD of $1\times10^{-12}\mathrm{g}^2/\mathrm{Hz}$,i.e., the RMS (root-mean-squared value) is 1% of the burying mode force. The modal forces of these two modes are correlated, with a coherence of 0.5. The simulated data is contaminated with i.i.d. Gaussian white noise with a PSD of $2.5\times10^{-11}\mathrm{g}^2/\mathrm{Hz}$. A set of synthetic data is generated for 1000s with a sampling frequency of 100Hz.

Figure 4 and Figure 5 show the (root) PSD and singular value spectrum of the data, respectively. It is difficult to detect the buried mode solely from the PSD spectrum. The spectral peak of the buried mode can be found as the second singular value in the plot of the singular value spectrum. The remaining singular values roughly reflect the noise level of the measured data. The two modes are well apart so a wide frequency band covering the spectral peaks of both modes is needed to identify modal parameters using conventional multi-mode algorithms. This is not necessary for the proposed method. Only the FFT points around the resonance peak of the buried mode are selected for modal identification. The frequency band selected to identify the buried mode in this example is [4.8 5.2]Hz.

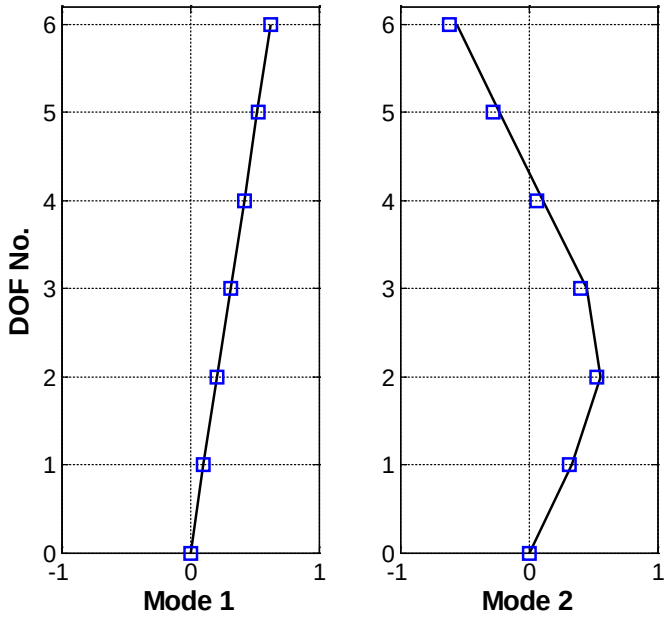

Figure 3. Mode Shapes, Synthetic Data Example (Solid Line: Exact; Square: MPV)

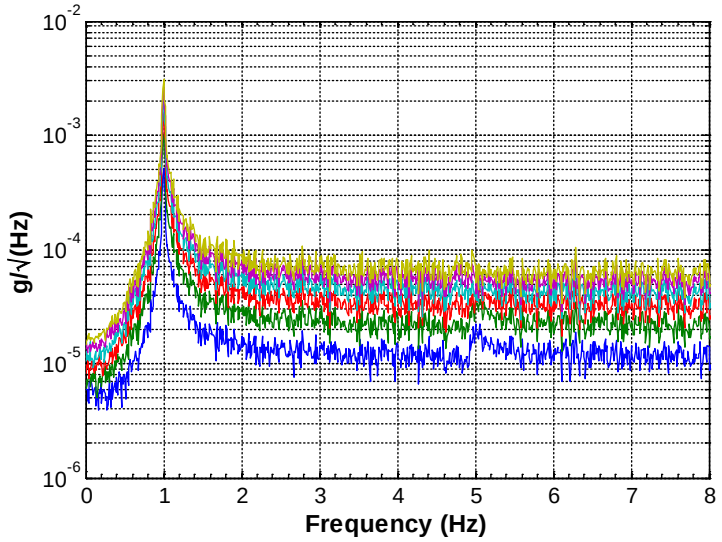

Figure 4. Root PSD Spectrum, Synthetic Data Example

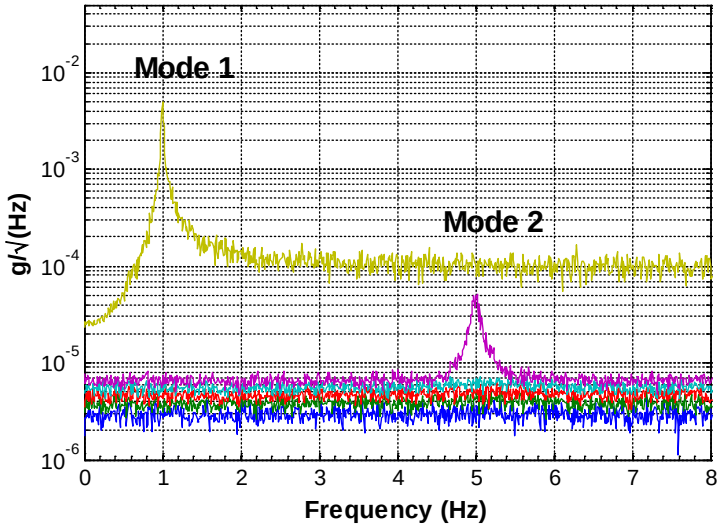

Figure 5. Root Singular Value Spectrum, Synthetic Data Example

Table 1. Identified Modal Parameters (MPV), Synthetic Data Example

Mode	f (Hz)		$\zeta(\%)$		$S\left(10^{-12}\mathrm{g}^2/\mathrm{Hz}\right)$		$S_e\left(10^{-11}\mathrm{g}^2/\mathrm{Hz}\right)$		χ	
	MPV	Exact	MPV	Exact	MPV	Exact	MPV	Exact	MPV	Exact
2	4.995	5.000	0.96	1.00	1.02	1.00	2.50	2.50	0.47	0.5

Table 1 lists the identified modal parameters based on the proposed method. It can be seen that the proposed method provides a good estimation on the modal parameters of the buried mode where the identified values are quite close to the exact ones. Figure 3 plots the identified mode shapes (squares) and the exact ones (solid lines). These two types of mode shapes almost coincide. The MAC (modal assurance criterion) values are calculated to be 0.9999 and 0.9949 for Mode 1 and 2, respectively. Although modal analysis focuses on the buried mode, the proposed method can also provide a good estimation on the mode shapes of the burying mode.

In addition to the MPVs, the associated uncertainty of the identified modal parameters has also been investigated. In a Bayesian context, the identification uncertainty can be quantitatively assessed through the posterior covariance matrix (whose square root of the diagonal entry gives the posterior standard deviation of the corresponding modal parameters), which is equal to the inverse of Hessian of the NLLF at MPV. In this test, the posterior covariance matrix is calculated using the finite difference method and the identification uncertainty are discussed based on the posterior coefficient of variation (i.e., c.o.v. =

posterior standard deviation / MPV). Specifically, the posterior c.o.v. of mode shape is given by the square root sum of the eigenvalues of the corresponding partition in the full posterior covariance matrix [33]. For comparison, synthetic data simulating the single mode case without the buring mode was generated and the identification uncertainty was calculated using [34]. Table 2 lists the identification uncertainty of the modal parameters for these two cases. The posterior c.o.v.s of the natural frequency and damping ratio of the buried mode are similar to the values in the single mode case, suggesting that the burying situation does not have much effect on the identification uncertainty of these two parameters. This is not the case for the mode shape, however. The posterior uncertainty of the mode shape for the buried mode is significantly larger than that for the single mode case.

Table 2. Identification Uncertainty of Modal Parameters

	Posterior c.o.v. (%)		
	Natural Frequency	Damping Ratio	Mode Shape
Buried Mode	0.07	7.6	16
Single Mode	0.06	8.9	1.3

6.2 Effect of PSD of modal force for the burying mode

In real applications, the ratio between the modal force PSD of the buried mode and that of the burying mode can be different. The spectral peak of the mode of interest can be partially buried by the burying mode or totally buried. In this example, such effect on the MPV and the identification quality of the mode of interest is investigated through a parametric study using synthetic data. Consider the same data configuration in Section 6.1 except for the modal force PSD of the burying mode. Six scenarios with increasing modal force PSD of the burying mode are considered, i.e. $1\times10^{-11}\text{g}^2/\text{Hz}$, $1\times10^{-10}\text{g}^2/\text{Hz}$, $1\times10^{-9}\text{g}^2/\text{Hz}$, $1\times10^{-8}\text{g}^2/\text{Hz}$, $1\times10^{-7}\text{g}^2/\text{Hz}$ and $1\times10^{-6}\text{g}^2/\text{Hz}$, giving the ratio of the modal force PSD between the two modes from 10 to 10^6. Figure 6 shows the root singular value spectrum for these six scenarios based on a typical data set, respectively. For the first three scenarios, the mode of interest is partially buried by the burying mode as its modal response at the resonance peak is still larger that the modal response of the burying mode. On the other hand, the mode of interest is fully buried by the burying mode in the last three scenarios. For each scenario, 1000 data sets are simulated to investigate the sample mean and variance of the identified modal parameters.

The sample mean of the identified natural frequencies and damping ratios of the buried mode among simulated data sets are calculated to be 5Hz and 1% respectively for all the scenarios, suggesting practically no bias in the MPV of these two parameters.

Table 3 lists the sample c.o.v of natural frequency and damping ratio MPVs of the buried mode among the simulated data sets. It should be noted that the sample c.o.v. investigated in this example is different from the posterior c.o.v. discussed in the previous example. The posterior c.o.v. is the unresolved uncertainty given measured data and model assumptions while the sample c.o.v. also involves the effect of modelling error. The ratio of modal force PSDs is the one between the modal force PSD of the burying mode and that of the buried mode. It can be seen that the sample c.o.v.s are of the same order of magnitude among different scenarios for both frequency and damping ratio. The PSD of modal force for the burying mode has little effect on the identification accuracy of these two parameters. This is not the case for the identified mode shapes, however. Figure 7 shows the sample mean of the mode shape MAC against the ratio of modal force PSDs. The MAC values are calculated between the identified mode shape and the exact mode shape that is used to generate synthetic data. It can be seen that the MAC values are close to one for the first four scenarios, suggesting good estimation quality on the identified mode shapes. However, there is a decrease in the MAC values for the last two cases. This indicates that when the modal force of the burying mode is several orders of magnitude larger than that of the buried mode, the mode shape of the buried mode cannot be well identified. This is reasonable as the mode shape value for a particular channel can only be identified based on the measured data within that channel. When the modal response of the burying mode is extremely large in some channels, the randomness in those channels will also be very high, which affects the estimation of the mode shape values for the buried mode.

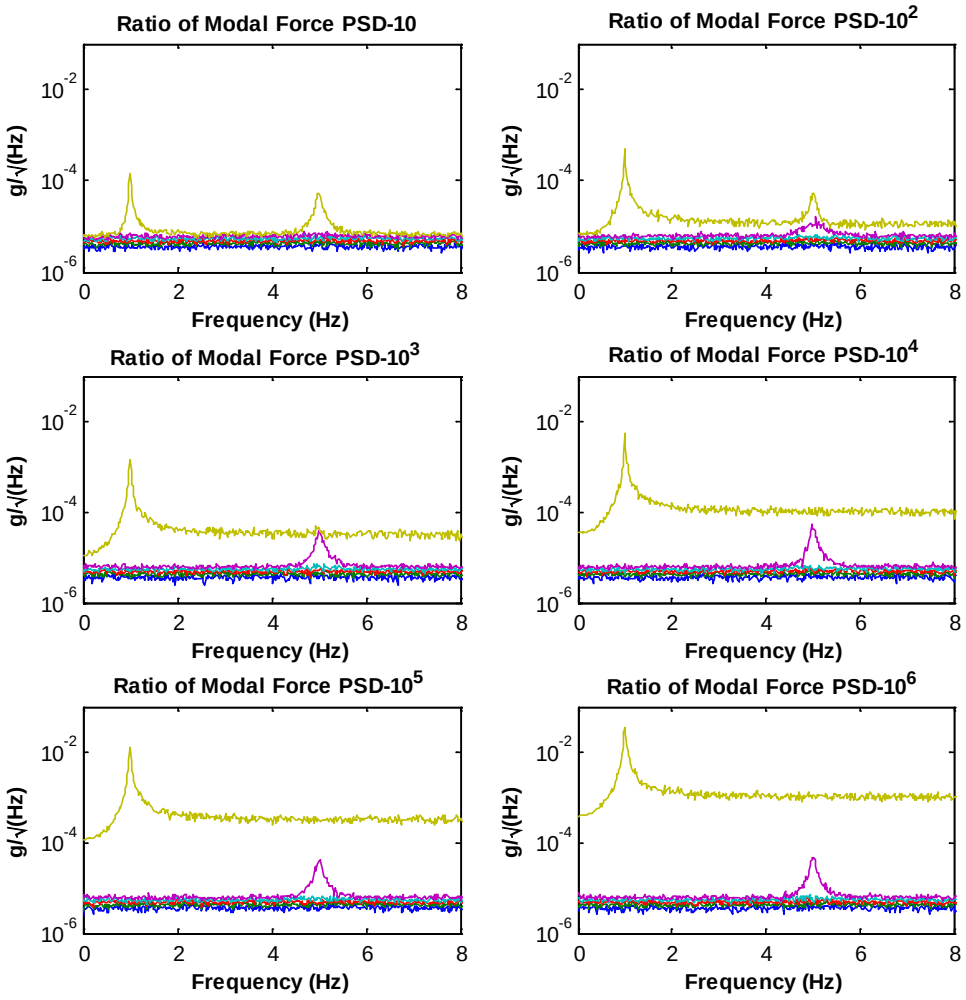

Figure 6. Root Singular Value Spectrum for The Six Scenarios

Table 3. Sample c.o.v.s of Natural Frequency and Damping Ratio MPVs (buried mode)

Modal Parameters	Ratio of Modal force PSDs					
	10	10^2	10^3	10^4	10^5	10^6
$f\left(1\times10^{-4}\right)$	10	8.7	8.3	8.0	7.9	8.5
$\zeta\left(1\times10^{-2}\right)$	8.6	7.3	7.5	7.5	7.2	7.5

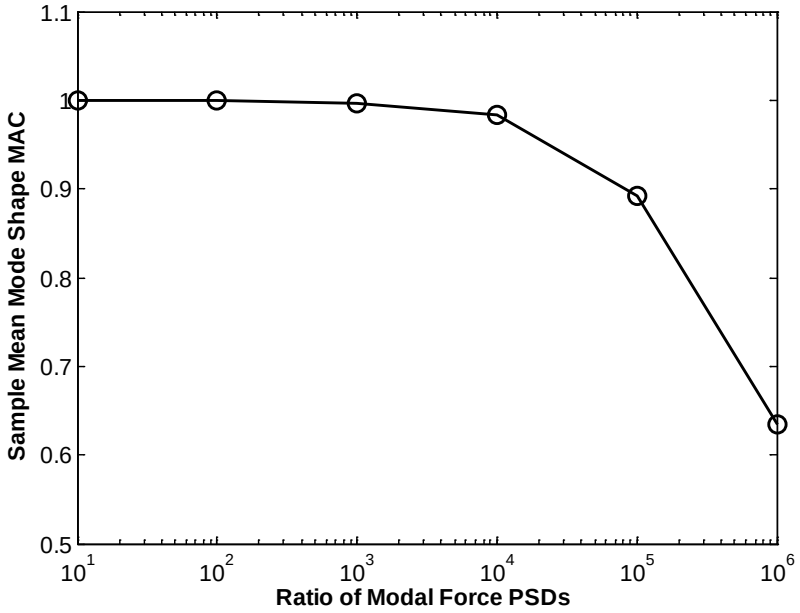

Figure 7. Sample Mean Mode Shape MAC against Ratio of Modal Force PSD (buried mode)

6.3 Jiangyin Yangtze River Bridge

The proposed method is applied to modal identification of the buried modes encountered in a full-scale ambient vibration test in this section. The instrumented structure is the Jiangyin Yangtze River Bridge (see Figure 8). It is a suspension bridge over the Yangtze River in Jiangsu, China. Figure 9 shows the front view of the bridge. The bridge has an overall length of 3km with a main span about 1.4km. The main deck of the bridge is 37m wide with a depth of 3m. It is used as a highway bridge with dual three-lane and hard shoulders. Detailed construction information about the bridge can be found in [35].

Figure 8. Jiangyin Yangtze River Bridge

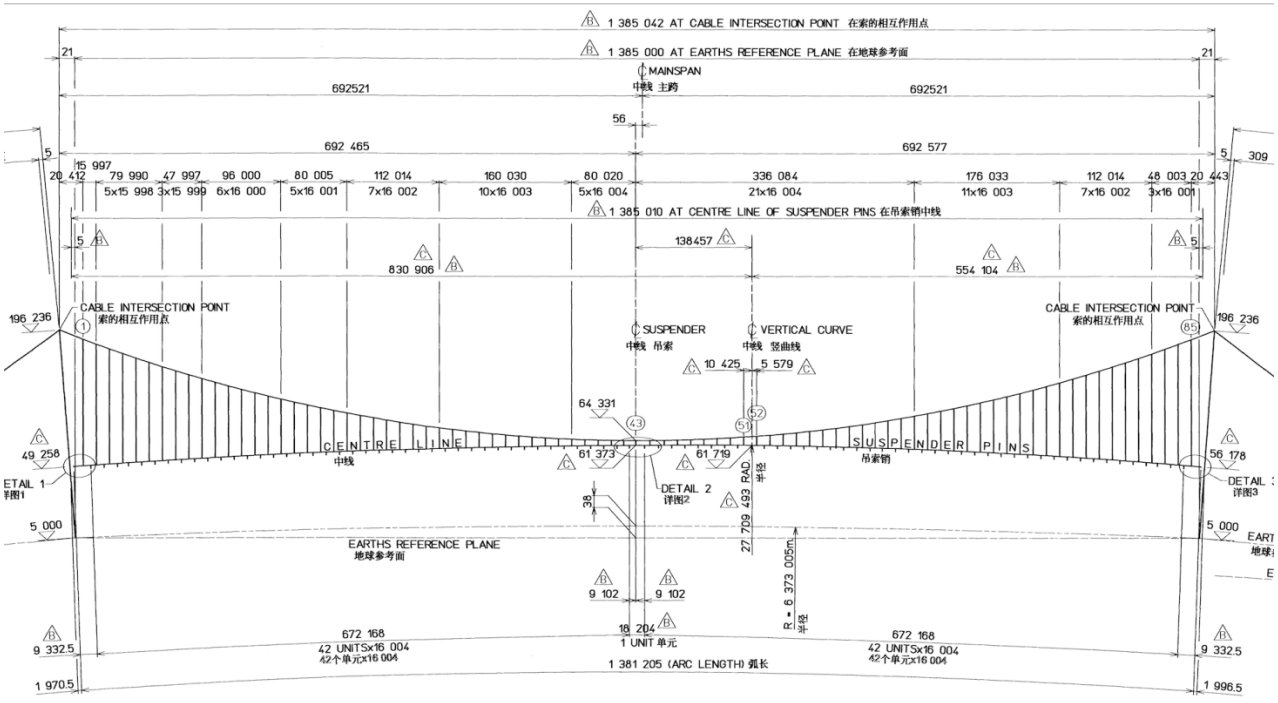

Figure 9. Elevation of Jiangyin Yangtze River Bridge

Ambient vibration tests were conducted on this bridge in April 2017. Eight uniaxial force-balanced accelerometers with three data acquisition (DAQ) units were used in the test. Figure 10 shows a set of equipment for each measurement location on site. Due to the limited number of sensors and DAQ units, multiple setups were conducted, roving from the south side to the north side of the bridge in order to capture the overall vibration pattern of the bridge. Most of the setups are conducted on the east side of the bridge deck with one on the west side (capturing the torsional modes) and three on the south tower (capturing the tower motion). For the measurement locations on the deck, the sensors were placed near the hanger with a spacing of 4 hangers (48m) between two locations. The vibration responses in vertical and transverse directions were measured (see Figure 10). For the setups on the bridge tower, the vibration responses were measured in transverse and longitudinal directions. Two reference locations near the south tower of the bridge were chosen in order to assemble the overall mode shapes of the bridge. Despite the reference locations, each setup covers two measurement locations with 13 setups in total (i.e., $(2\times13+2)\times2=56$ DOFs). One hour of ambient data was measured in each setup with a sampling frequency of 25.6Hz. See [36] for detailed field implementation and OMA of this test.

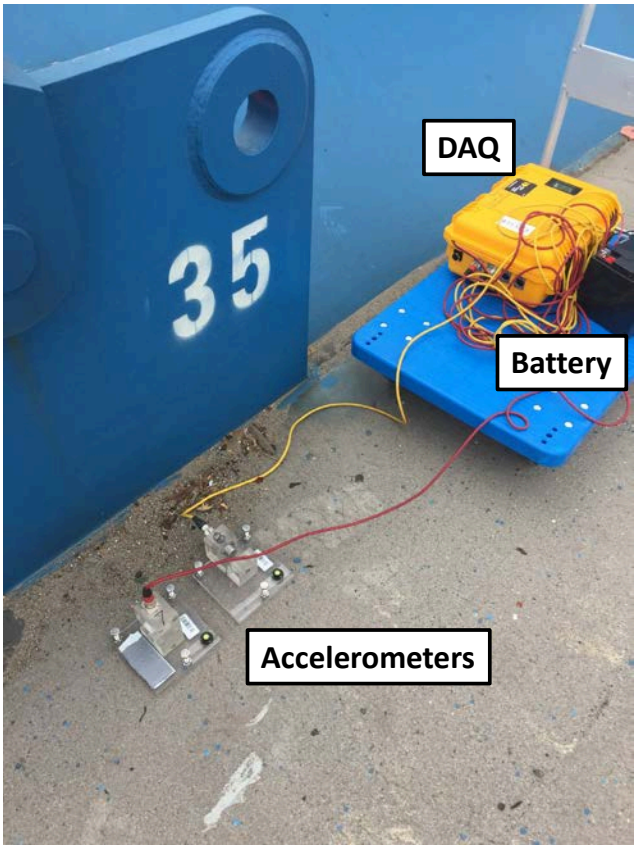

Figure 10. Equipment per Measurement Location on Site

Figure 1 (see Section 1) shows the (root) PSD spectrum of the measured data in the first setup. It can be seen that there are two groups of data with PSDs of different orders of magnitude. The upper plots (dashed lines) correspond to vertical direction and the lower ones (solid lines) correspond to the transverse direction. This is a typical situation in ambient vibration tests for long-span bridges as the traffic load (in the vertical direction) is normally much larger than the wind load (in the transverse direction). The corresponding root singular value spectrum is shown in Figure 11. Modal identification in this example focuses on two buried modes (indicated in the spectra) with natural frequency around 0.145Hz and 0.24Hz, respectively. Identification results based on the proposed method are investigated by comparing with those based on a wide band with two modes; and those based on a narrower band with a single mode using transverse channels only [24]. The overall mode shapes are assembled based on the identified mode shapes within individual setups using the global least square method [37].

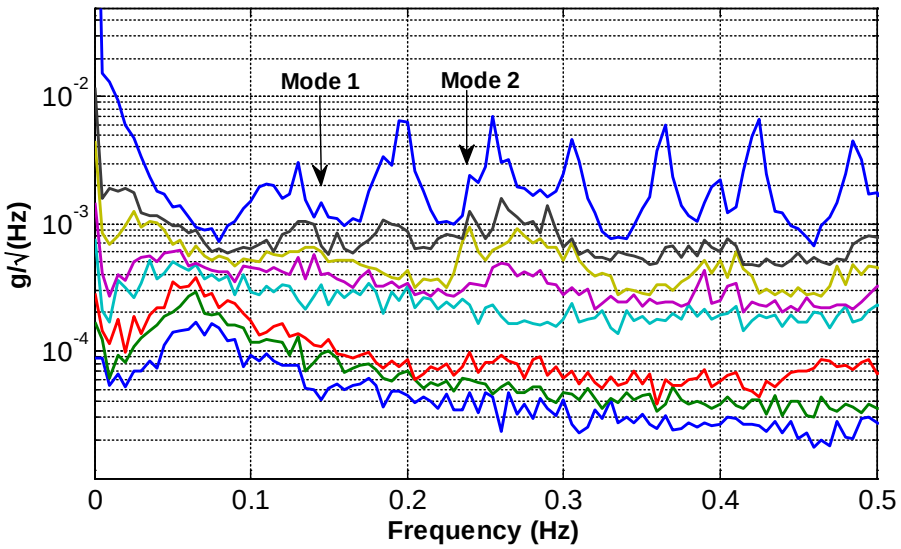

Figure 11. Root Singular Value Spectrum of Setup 1

Mode 1

Mode 1 is buried by the mode with a natural frequency about 0.13Hz on the left-hand side. It should be noted that in some setups, this mode is not fully buried (i.e., the spectral density of this mode at its resonance peak is higher than that of the mode on its left-hand side. In this context, the order of the initial guesses $\mathbf{B}'(1)$ and $\mathbf{B}'(2)$ (see Section 4.1) need to be swapped when forming the mode shape basis $\mathbf{B}'$ as the largest singular value now reflects the spectral properties of the buried mode instead of the burying mode.

Figure 13 shows the identified mode shape based on the proposed method; the conventional method assuming multiple modes (abbreviated as ‘multi-mode method’) and single mode (abbreviated as ‘single mode method’), respectively. The selected frequency band for the proposed method and single mode method is [0.14 0.16]Hz and that for the multi-mode method is [0.12 0.16]Hz (to involve the burying mode). It is a transverse mode with a modal node in the middle of the bridge. It can be seen that the assembled overall mode shapes based on these methods generally agree well with each other. Figure 12 shows the identified natural frequencies and damping ratios in individual setups for the proposed method and multi-mode method, where the dashed line represents the mean value among the setups. The identified values between these two methods are generally close to each other but discrepancies can be found in some setups, especially for the identified damping ratios. This is reasonable as they are actually identified based on the FFT data in different frequency bands where the wide band for the multi-mode method may involve more modelling error. For the single mode method, the mode shape values in the vertical direction are not identified and are set to zero in the plot. It can be seen that the transverse part of the identified mode shape based on the proposed method also agrees well with the one based on the single mode method.

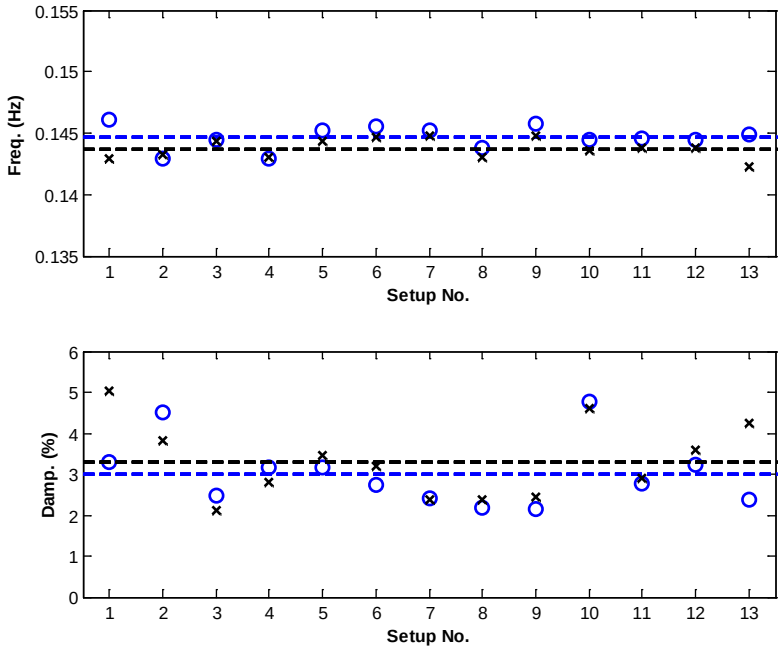

Figure 12. Identified Natural Frequency and Damping Ratio of Mode 1 Among Setups (Blue Circle: Proposed Method; Black cross: Multi-mode Method; Dashed Line: Mean Value)

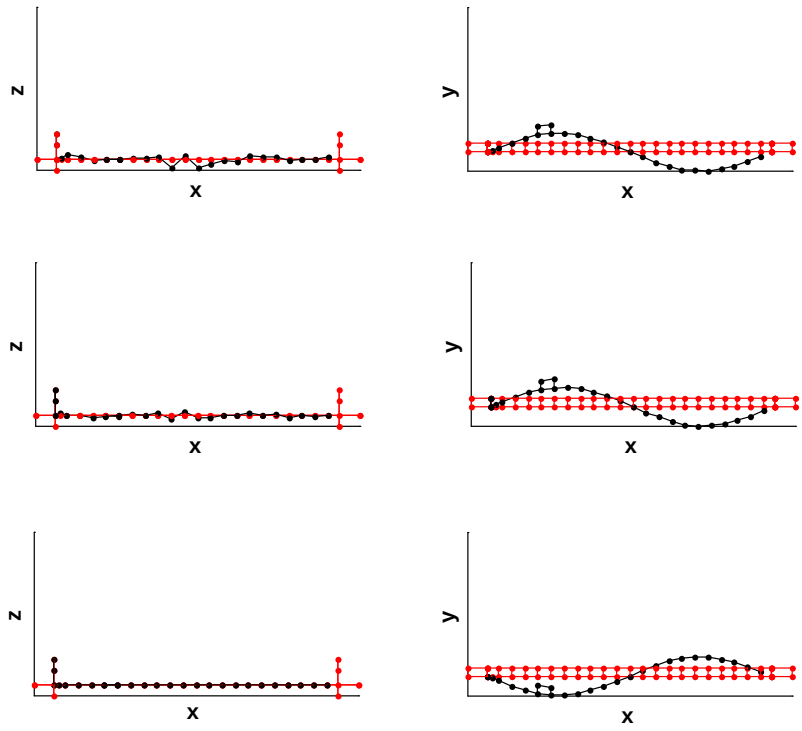

Figure 13. Identified Mode Shape of Mode 1, (a) Proposed Method (b) Multi-Mode Method (c) Single Mode Method

Mode 2

Figure 14 shows the identified mode shape of Mode 2 based on the proposed method and the single mode method, respectively, where the selected frequency band is [0.237 0.242]Hz. It is a mode swaying in both vertical and transverse directions, but with lopsided transverse motion. It is an unusual mode not commonly observed in other long-span bridges, even the asymmetric Humber Bridge [38]. There is also an element of torsion indicated by the two measurement points on the west side, as if the deck is swinging from the main cables. Assuming two modes with a wide band cannot give a reasonable estimation on the mode shapes for this mode as in some setups there are additional peaks between the mode of interest and the burying mode. Further analysis also reveals that these peaks are not global modes of the bridge. Figure 15 shows the root PSD spectrum of the fifth setup as a typical case. There is an additional peak in some data channels close to the second mode around 0.235Hz. The mode shape MPVs can be erroneously determined when these peaks occur in the selected frequency band. The identification process cannot even converge in some setups. Figure 14(b) shows the identified overall mode shape using the single mode method with

horizontal data channels only. Similar to the first mode, the identified mode shapes are close to those horizontal parts based on the proposed method. However, the vertical motion of this mode cannot be identified as only transversal data channels are used in modal identification in this case.

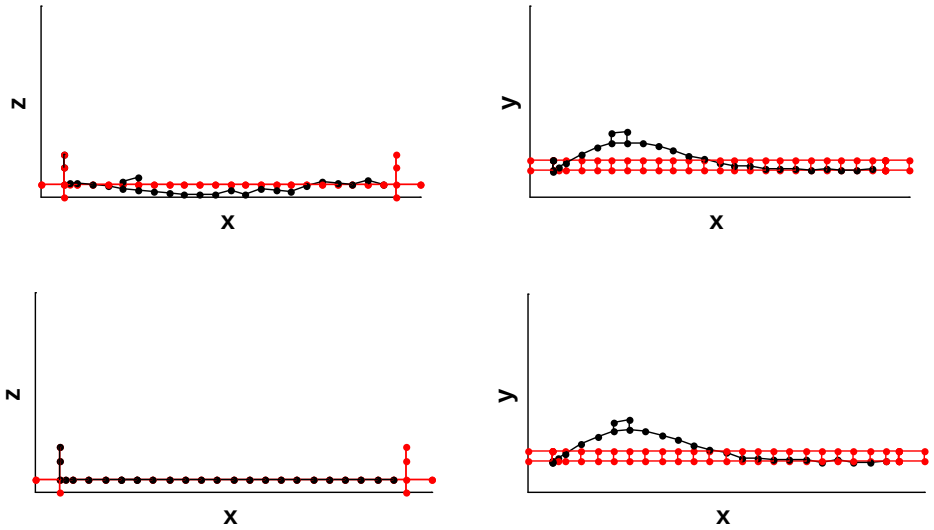

Figure 14. Identified Mode Shape of Mode 2 (a) Proposed Method (b) Single Mode Method

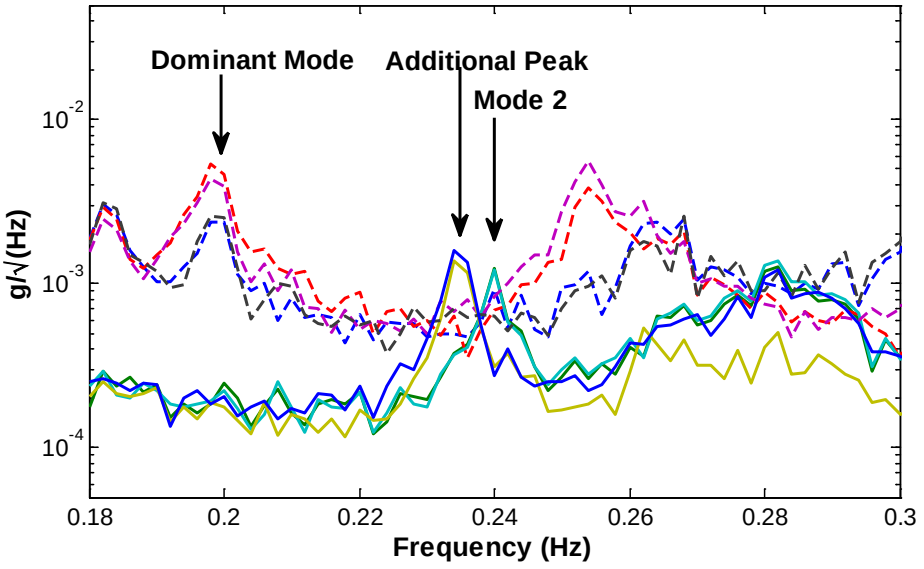

Figure 15. Root PSD Spectrum of Setup 5 (Dashed Line: Vertical Direction; Solid Line: Transverse Direction)

7. Conclusions

This paper has proposed a Bayesian modal identification method for buried modes based on ambient vibration data. Buried mode situation happens when the spectral response of a mode is significant around the resonance peak of the mode of interest. In this context, the spectral characteristics of the latter can be buried by the former within the frequency band of interest. Such a situation has been modelled around the resonance peak of the buried mode and the Bayesian modal identification formulation for the buried mode has been derived. Computational difficulties have been addressed and a fast iterative procedure has been proposed for efficient determination of MPVs of modal parameters. The proposed method has been validated using a synthetic data example. The example shows that the burying situation does not have a significant effect on the identification uncertainty of the natural frequency and damping ratio. However, the identified mode shape has much larger uncertainty compared to the single mode case. A parametric study illustrates that the proposed method can provide a good estimation of natural frequencies and damping ratios. The identification quality of mode shapes is also good unless the PSD of modal force for the burying mode is several orders of magnitude larger than that of the buried mode. The proposed method has been applied to modal identification of the buried modes in a full-scale ambient test. As seen in this example, the proposed method can provide a good estimation on the modal properties of buried modes under field test conditions. The proposed method involves reduced modelling error and computational effort as modal identification focuses on the FFT data around the resonance peak of the buried mode. Compared to conventional methods where only a subset of the data channels is used for modal identification, the mode shape values of the buried mode in all measured DOFs now can be identified using the proposed method. This provides an opportunity to gain more insights on the nature of buried modes, especially the mode shape. New information on bridge behaviour might be revealed by re-examination of data sets from long-span bridge investigations using traditional OMA procedures.

This paper mainly focuses on determining the MPV of modal parameters for buried mode situations. Deriving the analytical expressions of the posterior uncertainties for buried mode situations is also an important task in the development of OMA techniques, which can be one of the future works. In this paper, the proposed method only considers one burying mode and one buried mode. In practice, more complicated situation can be encountered with more than one buring mode or more than one buried mode within the frequency band of interest.

Bayesian OMA methods for such situation can be developed based on the general multiple mode algorithms but the relationship between the modes is much more complicated. For example, one mode can be buried by another mode while it can also bury the third mode. In this case, whether this mode should be considered as the burying mode or buried mode depends on the mode of interest and different assumptions and models should be applied. Further development based on this issue can be challenging but the resulting method will be useful in practice.

Acknowledgement

This paper is partially supported by Tung Doctoral Scholarship and UK Engineering & Physical Research Council (EP/N017897/1 and EP/N017803). The financial support is gratefully acknowledged.

References

[1] R. Brincker, C.E. Ventura, Introduction to Operational Modal Analysis, Wiley, London, 2015. doi:10.1002/9781118535141.

[2] H. Wenzel, D. Pichler, Ambient vibration monitoring, Wiley, UK, 2005.

[3] L. Hermans, H. Van Der Auweraer, Modal Testing and Analysis of Structures Under Operational Conditions: Industrial Applications, Mech. Syst. Signal Process. 13 (1999) 193–216. doi:10.1006/mssp.1998.1211.

[4] F.N. Catbas, T. Kijewski-Correa, A.E. Aktan, Structural identification (St-Id) of constructed facilities: Approaches, methods and technologies for effective practice of St-Id, in: Am Soc Civ Eng, 2011.

[5] A.M. Abdel-Ghaffar, R.H. Scanlan, Ambient vibration studies of Golden Gate bridge: 1. Suspended structure, and 2. Pier tower structure, ASCE J. Eng. Mech. 111 (1985) 463–482. doi:10.1061/(ASCE)0733-9399(1985)111:4(463).

[6] K.Y. Koo, J.M.W. Brownjohn, D.I. List, R. Cole, Structural health monitoring of the Tamar suspension bridge, Struct. Control Heal. Monit. 20 (2013) 609–625. doi:10.1002/stc.1481.

[7] J.P. Lynch, Y. Wang, K.J. Loh, J.-H. Yi, C.-B. Yun, Performance monitoring of the

Geumdang Bridge using a dense network of high-resolution wireless sensors, Smart Mater. Struct. 15 (2006) 1561–1575. doi:10.1088/0964-1726/15/6/008.

[8] J.-H. Weng, C.-H. Loh, J.P. Lynch, K.-C. Lu, P.-Y. Lin, Y. Wang, Output-only modal identification of a cable-stayed bridge using wireless monitoring systems, Eng. Struct. 30 (2008) 1820–1830. doi:10.1016/j.engstruct.2007.12.002.

[9] Y.Q. Ni, B. Li, K.H. Lam, D.P. Zhu, Y. Wang, J.P. Lynch, K.H. Law, In-construction vibration monitoring of a super-tall structure using a long-range wireless sensing system, Smart Struct. Syst. 7 (2011) 83–102. doi:10.12989/sss.2011.7.2.083.

[10] Q.S. Li, Y.Q. Xiao, J.R. Wu, J.Y. Fu, Z.N. Li, Typhoon effects on super-tall buildings, J. Sound Vib. 313 (2008) 581–602. doi:10.1016/j.jsv.2007.11.059.

[11] J.Y. Fu, Q.S. Li, J.R. Wu, Y.Q. Xiao, L.L. Song, Field measurements of boundary layer wind characteristics and wind-induced responses of super-tall buildings, J. Wind Eng. Ind. Aerodyn. 96 (2008) 1332–1358. doi:10.1016/j.jweia.2008.03.004.

[12] S.-K. Au, F.-L. Zhang, P. To, Field observations on modal properties of two tall buildings under strong wind, J. Wind Eng. Ind. Aerodyn. 101 (2012) 12–23. doi:10.1016/j.jweia.2011.12.002.

[13] I. James, George H., T.G. Carne, J.P. Lauffer, The natural excitation technique (NExT) for modal parameter extraction from operating structures, Int. J. Anal. Exp. Modal Anal. 10 (1995) 260–277.

[14] B. Peeters, G. De Roeck, Reference-Based Stochastic Subspace Identification for Output-Only Modal Analysis, Mech. Syst. Signal Process. 13 (1999) 855–878. doi:10.1006/mssp.1999.1249.

[15] P. Van Overschee, B.L. De Moor, Subspace identification for linear systems: Theory—Implementation—Applications, Springer Science & Business Media, 2012.

[16] R. Brincker, L. Zhang, P. Andersen, Modal identification of output-only systems using frequency domain decomposition, Smart Mater. Struct. 10 (2001) 441–445. doi:10.1088/0964-1726/10/3/303.

[17] K.V. Yuen, L.S. Katafygiotis, Bayesian time-domain approach for modal updating using ambient data, Probabilistic Eng. Mech. 16 (2001).

[18] L.S. Katafygiotis, K.V. Yuen, Bayesian spectral density approach for modal updating using ambient data, Earthq. Eng. Struct. Dyn. 30 (2001) 1103–1123. doi:10.1002/eqe.53.

[19] W.-J. Yan, L.S. Katafygiotis, A two-stage fast Bayesian spectral density approach for ambient modal analysis. Part I: Posterior most probable value and uncertainty, Mech. Syst. Signal Process. 54 (2015) 139–155. doi:10.1016/j.ymssp.2014.07.027.

[20] W.-J. Yan, L.S. Katafygiotis, A two-stage fast Bayesian spectral density approach for ambient modal analysis. Part II: Mode shape assembly and case studies, Mech. Syst. Signal Process. 54 (2015) 156–171. doi:10.1016/j.ymssp.2014.08.016.

[21] K.V. Yuen, L.S. Katafygiotis, Bayesian fast Fourier transform approach for modal updating using ambient data, Adv. Struct. Eng. 6 (2003) 81–95.

[22] S.-K. Au, F.-L. Zhang, Y.-C. Ni, Bayesian operational modal analysis: Theory, computation, practice, Comput. Struct. 126 (2013) 3–14. doi:10.1016/j.compstruc.2012.12.015.

[23] S.-K. Au, Operational Modal Analysis: Modeling, Bayesian Inference, Uncertainty Laws, Springer, 2017.

[24] S.-K. Au, Fast Bayesian ambient modal identification in the frequency domain, Part I : Posterior most probable value, Mech. Syst. Signal Process. 26 (2012) 60–75. doi:10.1016/j.ymssp.2011.06.017.

[25] D.R. Brillinger, Time series: data analysis and theory, Siam, 1981.

[26] J.L. Beck, L.S. Katafygiotis, Updating Models and Their Uncertainties. I: Bayesian Statistical Framework, J. Eng. Mech. 124 (1998) 455–461. doi:10.1061/(ASCE)0733-9399(1998)124:4(455).

[27] Z. Wen, W. Yin, A feasible method for optimization with orthogonality constraints, Math. Program. 142 (2013) 397–434. doi:10.1007/s10107-012-0584-1.

[28] J. Crank, P. Nicolson, A practical method for numerical evaluation of solutions of partial differential equations of the heat-conduction type, Math. Proc. Cambridge Philos. Soc. 43 (1947) 50–67. doi:10.1017/S0305004100023197.

[29] S. Friedland, J. Nocedal, M.L. Overton, The formulation and analysis of numerical methods for inverse eigenvalue problems, SIAM J. Numer. Anal. 24 (1987) 634–667.

[30] S. Patankar, Numerical heat transfer and fluid flow, 1980. doi:10.1016/j.watres.2009.11.010.

[31] D. Goldfarb, Z. Wen, W. Yin, A curvilinear search method for p-Harmonic Flows on Spheres, SIAM J. Imaging Sci. (2009). doi:10.1137/080726926.

[32] J. Barzilai, J.M. Borwein, Two-point step size gradient methods, IMA J. Numer. Anal. 8 (1988) 141–148. doi:10.1093/imanum/8.1.141.

[33] S.-K. Au, F.-L. Zhang, On assessing the posterior mode shape uncertainty in ambient modal identification, Probabilistic Eng. Mech. 26 (2011) 427–434. doi:10.1016/j.probengmech.2010.11.009.

[34] S.-K. Au, Fast Bayesian ambient modal identification in the frequency domain, Part II: Posterior uncertainty, Mech. Syst. Signal Process. 26 (2012) 76–90. doi:10.1016/j.ymssp.2011.06.019.

[35] J. Young, Jiangyin Yangtze River Bridge, China, Bridg. Eng. 156 (2003) 45–53. doi:10.1680/bren.156.1.45.37150.

[36] J.M.W. Brownjohn, S.-K. Au, Y.-C. Zhu, Z. Sun, B.-B. Li, J. Bassitt, D.E. Hudson, H. Sun, Bayesian operational modal analysis of Jiangyin Yangtze River Bridge, Mech. Syst. Signal Process. 110 (2018) 210–230. doi:10.1016/j.ymssp.2018.03.027.

[37] S.-K. Au, Assembling mode shapes by least squares, Mech. Syst. Signal Process. 25 (2011) 163–179. doi:10.1016/j.ymssp.2010.08.002.

[38] J.M.W. Brownjohn, F. Magalhães, E. Caetano, A. Cunha, Ambient vibration re-testing and operational modal analysis of the Humber Bridge, Eng. Struct. 32 (2010) 2003–2018. doi:10.1016/j.engstruct.2010.02.034.